BIOCHEMISTRY
including biophysical chemistry & molecular biology

Article

pubs.acs.org/biochemistry

High Stability and Cooperative Unfolding of α-Synuclein Oligomers

Wojciech Paslawski,[†,‡] Maria Andreasen,[†,‡] Søren Bang Nielsen,[†,‡,∥] Nikolai Lorenzen,[†,‡,⊥] Karen Thomsen,[†] Jørn Døvling Kaspersen,[†,§] Jan Skov Pedersen,[†,§] and Daniel E. Otzen*[,†,‡]

[†]Interdisciplinary Nanoscience Center (iNANO), Aarhus University, Gustav Wieds Vej 14, DK − 8000 Aarhus C, Denmark
[‡]Department of Molecular Biology and Genetics, Aarhus University, Gustav Wieds Vej 10C, DK − 8000 Aarhus C, Denmark
[§]Department of Chemistry, Aarhus University, Langelandsgade 140, DK − 8000 Aarhus C, Denmark

ABSTRACT: Many neurodegenerative diseases are linked with formation of amyloid aggregates. It is increasingly accepted that not the fibrils but rather oligomeric species are responsible for degeneration of neuronal cells. Strong evidence suggests that in Parkinson's disease (PD), cytotoxic α-synuclein (αSN) oligomers are key to pathogenicity. Nevertheless, insight into the oligomers' molecular properties remains scarce. Here we show that αSN oligomers, despite a large amount of disordered structure, are remarkably stable against extreme pH, temperature, and even molar amounts of chemical denaturants, though they undergo cooperative unfolding at higher denaturant concentrations. Mutants found in familial PD lead to slightly larger oligomers whose stabilities are very similar to that of wild-type αSN. Isolated oligomers do not revert to monomers but predominantly form larger aggregates consisting of stacked oligomers, suggesting that they are off-pathway relative to the process of fibril formation. We also demonstrate that 4-(dicyanovinyl)julolidine (DCVJ) can be used as a specific probe for detection of αSN oligomers. The high stability of the αSN oligomer indicates that therapeutic strategies should aim to prevent the formation of or passivate rather than dissociate this cytotoxic species.

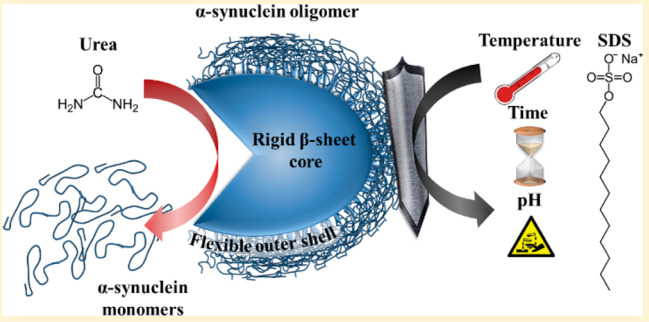

Neurodegenerative diseases (NDs) are often connected with formation of amyloid fibrils.[1] However, cytotoxic oligomeric species are increasingly seen as the main culprits in NDs like Parkinson's disease (PD),[2−5] Alzheimer's disease,[6−9] and tauopathies.[10] These soluble oligomers disrupt membranes possibly leading to neuronal damage.[3,11] Their role in the fibrillization process is complex. In some cases they seem to be directly engaged in assembly of fibrils, either as direct building blocks[12,13] or as nuclei that can be further elongated by monomeric species.[14−19] But they can also act as off-pathway species not directly involved in fibril formation.[20−25]

PD is one of the most widespread neurodegenerative disorders. The main component of PD-associated oligomers is α-synuclein (αSN), a presynaptic protein that plays a central role in disease.[26] The αSN point mutations A30P, E46K, H50Q, G51D, and A53T, together with the duplication or triplication of the gene coding for αSN,[27−33] are responsible for familial forms of PD. αSN has been proposed to facilitate the exocytosis and regulation of the synaptic vesicle trafficking[34] or take part in neurite outgrowth and adhesion of brain cells,[35,36] but its role in the neuronal cells remains unclear. Despite recent controversy,[37−42] it is still generally accepted that αSN has no persistent structure in the monomeric state under physiological conditions.[43] As mentioned, αSN can also self-associate into oligomeric species[2−5] and amyloid fibrils.[44,45] The well-documented cytotoxicity of the oligomeric species of αSN[5,46−51] has been suggested to derive from the formation of a pore-like structure, which disrupts the neuronal membrane.[2,11,49,52−54] The compelling evidence that these oligomers are key players in PD makes them promising targets for therapies against disease.[44,55−57] The oligomers' transient nature and intrinsic structural polydispersity are a challenge to high-resolution structural studies.[58,59] Recently we have used small-angle X-ray scattering (SAXS) to show that αSN oligomers can be described as a core surrounded by a halo of disorganized structure,[25] while our hydrogen/deuterium exchange mass spectrometry efforts have highlighted residues 39−75 as the most protected region.[60] Furthermore, this work identified two coexisting oligomers, of which the major species (accounting for around 80% of the entire oligomer population) does not readily exchange with monomers and is unable to form fibrils, consistent with independent kinetic studies.[25] The minor oligomeric species is in dynamic exchange with monomers and is proposed to form fibrils, but its small population and dynamic exchange properties make it difficult to detect in ensemble measurements.

Also, we have recently demonstrated that these αSN oligomers induce cytotoxicity in a rat brain cell line[61] where we have linked the cytotoxicity with the oligomers' ability to interact with and permeabilize membranes.[2,61,62]

Received: June 24, 2014
Revised: August 21, 2014
Published: September 12, 2014

   dx.doi.org/10.1021/bi5007833 | *Biochemistry* 2014, 53, 6252−6263

Here we analyze oligomers of wild-type (wt) and mutant αSN formed under fibrillization conditions.[2] Although we cannot separate the two types of oligomers by conventional means, our data will predominantly reflect the properties of the stable oligomer, which is by far the dominant species for both wild-type αSN and mutants.[25] We elucidate the structure, stability, and appearance of these oligomers in the fibrillization process by size-exclusion chromatography (SEC), dynamic light scattering (DLS), sodium dodecyl sulfate polyacrylamide gel electrophoresis (SDS-PAGE), transmission electron microscopy (TEM), SAXS, circular dichroism (CD), and fluorescence spectroscopy. Further, we report that 4-(dicyanovinyl)-julolidine (DCVJ), previously used for detection of prefibrillar aggregates of TTR,[63] is able to bind αSN oligomers resulting in significantly higher fluorescence signal than for monomers and fibrils. For both wt and mutant αSN, the formed oligomers are very stable and resist both extreme temperature and extreme pH; only high urea concentrations dissociate them to monomers. Prolonged incubation of oligomers leads to an increase in their size and formation of larger nonfibrillar aggregates.

MATERIALS AND METHODS

Materials. Unless stated otherwise, all chemicals were from Sigma Chemical Co. (St. Louis, MO) and were of analytical grade. All solutions were prepared using deionized water (Millipore, Milli-Q).

Preparation of αSN. αSN was expressed recombinantly in *E. coli* and purified as described.[64,65] For all experiments, fresh samples were prepared by dissolving lyophilized αSN in phosphate saline buffer (PBS) (20 mM phosphate, 150 mM NaCl, pH 7.4) and filtered (0.2 μm) prior to use. The concentration was determined with a NanoDrop (ND-1000, Thermo Scientific, USA) using a theoretical extinction coefficient of 0.412 $(mg/mL)^{-1}$ cm^{-1}.

Plate Reader Fibrillization of αSN. αSN wt, A30P, E46K, and A53T were fibrillated at a final concentration of 12 mg/mL with 40 μM thioflavin T (ThT) or 40 μM 4-(dicyanovinyl)-julolidine (DCVJ) in a Tecan Infinite Pro (Tecan Nordic AB) plate reader at 37 °C with 10 min shaking every 12 min as described.[66] Both ThT and DCVJ fluorescence were monitored by excitation at 448 nm and emission at 485 nm.

Purification of Oligomer. αSN oligomers were prepared as described.[2] Briefly, αSN was dissolved at 12 mg/mL in PBS buffer (20 mM phosphate, 150 mM NaCl, pH 7.4) and incubated in a Thermo-Shaker (TS-100, BioSan, Latvia) at 37 °C at 900 rpm for 5 h. Insoluble material was removed by centrifugation for 10 min at 12000*g*. Soluble fractions were loaded on a Superose 6 SEC column (Superose 6 XK 26/100) connected to an ÄKTA Basic system (GE Healthcare, USA) and eluted with PBS buffer at a 3 mL/min flow rate. Oligomer fractions were collected and stored at 4 °C. Note that the preparation of αSN oligomers was remarkably independent of protein concentration. Performing the preparation at 1 mg/mL αSN yielded oligomers indistinguishable in size, shape, and relative yield from those prepared at 12 mg/mL.[25]

DCVJ Fluorescence. DVCJ stock solution (5 mM dissolved in 100% ethanol) was mixed to a final concentration of 10 μM with 10 μM αSN monomer, oligomer, or fibril. DCVJ fluorescence emission spectra were recorded from 480 to 650 nm with excitation at 470 nm, 10 nm slit widths, and a scan speed of 200 nm/min on a LS55 luminescence spectrophotometer (PerkinElmer). Three spectra were accumulated and averaged for each sample.

Fourier Transform Infrared (FTIR) Spectroscopy. FTIR spectroscopy was performed using a Tensor27 FTIR spectrometer (Bruker) equipped with attenuated total reflection accessory with a continuous flow of N_2 gas. All samples were dried with N_2 gas. Sixty-four interferograms were accumulated at a spectral resolution of 2 cm^{-1} in the range from 1000 to 3998 cm^{-1}. Peak positions were assigned where the second order derivative had local minima and the intensity was modeled by Gaussian curve fitting using the OPUS 5.5 software. For comparison, all absorbance spectra are normalized.

Size-Exclusion Chromatography (SEC). The αSN oligomer was analyzed with a Postnova AF2000 flow field-flow fractionation system (Postnova Analytics GmbH, Germany) operating in SEC mode and equipped with a UV/vis (S3240) detector, Brookhaven BI-MwA molecular weight analyzer (measuring scattering intensity at 30°, 50°, 75°, 90°, 105°, 130°, and 145° angles), and PN3140 refractive index detectors (detectors listed in flow order). The analysis was carried out using a Superose 6 10/30 GL SEC column at a flow rate of 0.5 mL/min.

The appearance of the oligomer was monitored by loading 20 μL of 12 mg/mL αSN sample incubated for various amounts of time at 37 °C in an eppendorf shaker at 900 rpm. To remove fibrillar species, the sample was centrifuged for 10 min at 13000 rpm prior to analysis, and only the supernatant was loaded on the column.

αSN oligomer stability was monitored by loading 100 μL 0.2 mg/mL αSN oligomer sample at various incubation times at 37 °C using an autosampler.

Far-UV CD Spectroscopy. Far-UV wavelength spectra from 250 to 190 nm of 0.14 mg/mL αSN oligomers before and after heating to 120 °C using a 2 mm quartz cuvette were recorded with a Jasco J-810 spectrophotometer (Jasco Spectroscopic Co. Ltd., Japan). Scans were conducted at 20 °C with a step size of 0.2 nm, bandwidth 2 nm, and scan speed of 50 nm/min. Five spectra were averaged for each sample, and the buffer spectrum was subtracted. To examine the thermal stability, αSN monomers, oligomers, and fibrils at a concentration of 0.3 mg/mL (21 μM) were used in a 1 mm cuvette. Scans were conducted at 25 °C. Wavelength spectra were recorded from 20 to 95 °C with a 2 °C step increase. Fibril solutions were sonicated for 3 × 10 s at 50% power on ice with an HD 2070 Bandelin Sonuplus sonicator (Buch and Holm).

Membrane Permeabilization Assay. αSN oligomers at varying concentrations were mixed with dioleoylphosphatidylglycerol (DOPG) large unilamellar vesicles (LUV's) with a diameter of ∼100 nm, prepared by extrusion as described.[67] The fluorophore calcein was entrapped at self-quenching concentrations (70 mM) inside the vesicles; upon membrane permeabilization, calcein leaks from the vesicles, and this dilution increases its fluorescence response. Calcein release was measured in a 96-well-plate (Nunc, Thermo Fischer Scientific, Roskilde, Denmark) in duplicates. Calcein release was measured (excitation 485 nm; emission 520 nm) for 1 h in a Genios Pro fluorescence plate reader (Tecan, Mänerdorf, Switzerland) at 37 °C with 2 s shaking every 2 min. The calcein release percentage was calculated based on background fluorescence and 100% calcein release (addition of 0.2% (w/V) Triton X-100).

dx.doi.org/10.1021/bi5007833 | *Biochemistry* 2014, 53, 6252−6263

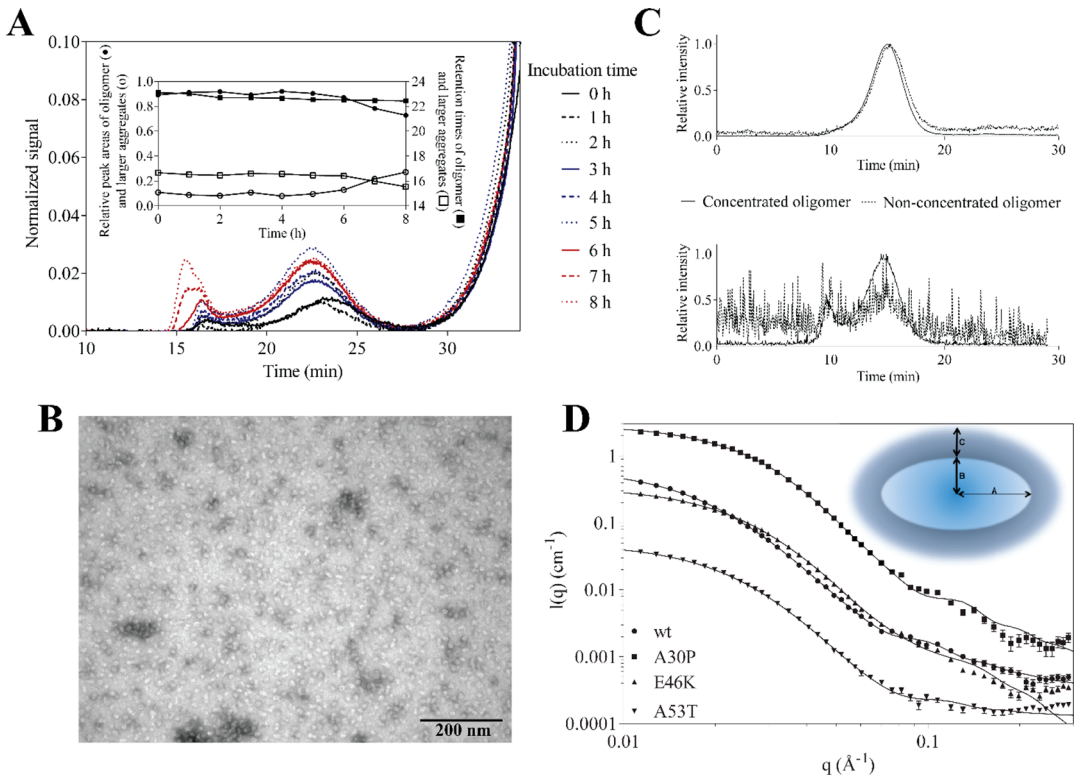

Figure 1. Size and shape of αSN oligomers. (A) Appearance of oligomer during the first few hours of fibrillation process analyzed by SEC. (Inset) Quantification of observed aggregates. Initially only oligomers and small amount of larger aggregates are observed, but after approximately 6 h, the quantity of larger aggregates start to increase. (B) TEM image of αSN oligomers, showing round structures with diameter of approximately 13 nm. (C) SEC-MALS analysis of the concentration step on αSN oligomers. (top) Absorbance at 214 nm. (bottom) Backscattering signal at 90°. (D) SAXS data fitted to the proposed model (of wt, A30P, E46K, and A53T αSN oligomers). There is no significant difference in the structure of oligomers formed by different variants of αSN. (Inset) SAXS based model of αSN oligomer. *A* and *B* are the dimensions of the rigid oligomer's core, which has an ellipsoidal shape with axis (*A*,*B*,*B*), while *C* represents the thickness of the flexible outer region of structure.

SDS-PAGE. The protein sample was mixed with 6× reducing sample buffer (375 mM Tris-HCl pH 6.8, 6% SDS, 50% glycerol, 9% β-mercaptoethanol, and 0.03% bromophenol blue) at a sample/buffer ratio of 5:1. The mixture was vortexed and then boiled at 100 °C for 5 min. The samples were loaded onto a bis-tris acrylamide gel (5%/15% stacking/running gel). Electrophoresis was performed using a vertical electrophoresis gel apparatus at a constant voltage of 140 V. The run was stopped when the dye front reached the bottom edge of the gel. The gel was stained using CBB R-250 solution (0.1% CBB R-250/40% methanol/10% glacial acetic acid) and destained using 4%/4% glacial acetic acid/ethanol solution. SDS-PAGE gels were scanned using standard table-top scanner or Typhoon Scanner (9400, GE Healthcare, USA). The intensity of protein bands was analyzed using ImageJ.[68]

Urea Dissociation of αSN Oligomers. Concentrated urea solutions in water were prepared and then adjusted to desired concentrations with water and 10× concentrated PBS buffer (200 mM phosphate, 1500 mM NaCl, pH 7.4). Protein samples (84 μM) were diluted into urea solutions of known concentrations and incubated for 1 h. Subsequently, samples were mixed with reducing gel loading buffer and analyzed by SDS-PAGE.

Urea Dissociation of αSN Oligomers Monitored by DCVJ Fluorescence. DVCJ was mixed with αSN oligomer to final concentrations of 10 μM DCVJ and 84 μM αSN, diluted into urea solutions of known concentrations, and incubated for 1 h. The fluorescence emission spectra were measured from 480 to 650 nm with excitation at 470 nm, 10 nm slit widths, and a scan speed of 200 nm/min. Three spectra were accumulated and averaged for each sample. Concentrated urea solutions in water were prepared and adjusted to the desired concentration with water and 10× concentrated PBS buffer (200 mM phosphate, 1500 mM NaCl, pH 7.4).

Fitting of Dissociation Curves. SDS-PAGE band intensity was normalized within each gel. Fluorescence spectra were parametrized by calculating an average emission wavelength, $\langle\lambda\rangle$,[69] defined as

$$\langle\lambda\rangle = \frac{\sum(\lambda_i F_i)}{\sum(F_i)} \quad (1)$$

λ_i and F_i are the emission wavelength and the corresponding fluorescence intensity, respectively, at the *i*th measuring point. The dissociation curves were fitted to a two-state model[70,71] using Kaleidagraph 4.0:

$$\text{signal} = \frac{S_M + S_O 10^{(m_{O-M}(-[\text{den}]^{50\%}+[\text{urea}]))}}{1 + 10^{(m_{O-M}(-[\text{den}]^{50\%}+[\text{urea}]))}} \quad (2)$$

Here S_M and S_O are the average signals of the monomeric and oligomeric states, $[\text{den}]^{50\%}$ is the denaturant concentration for which the fractions of folded and unfolded states are equal, and m_{O-M} is the slope of dissociation curve. The equations assume a linear relationship between the logarithm of the equilibrium constant ($K_{O-M}^{\text{denaturant}}$) and the denaturant concentration:

dx.doi.org/10.1021/bi5007833 | *Biochemistry* 2014, 53, 6252−6263

Table 1. SAXS Analysis of Dimensions and Flexibility of wt, A30P, E46K, and A53T αSN Oligomers

	dimensions (nm)				
αSN variant	A	B	C	flexible fraction	number of monomers per oligomer
wt	10.3 ± 0.3	4.0 ± 0.1	4.3 ± 0.1	0.57 ± 0.01	32.7
E46K	11.0 ± 0.1	4.1 ± 0.1	4.2 ± 0.2	0.53 ± 0.02	27.3
A30P	11.9 ± 0.1	4.4 ± 0.1	5.0 ± 0.4	0.51 ± 0.03	33.9
A53T	12.0 ± 0.1	4.8 ± 0.1	5.1 ± 0.4	0.45 ± 0.02	32.7

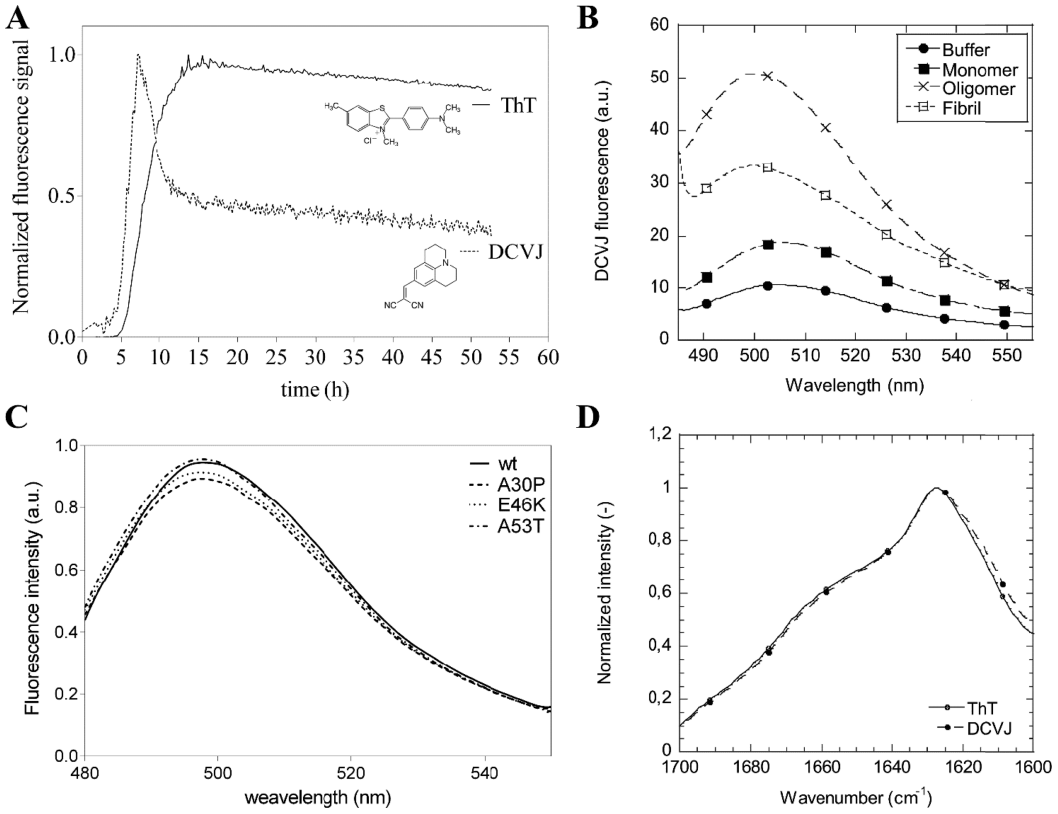

Figure 2. DCVJ binding to αSN species. (A) αSN fibrillation followed by ThT and DCVJ, showing the binding of DCVJ to intermediate αSN species. Structures of ThT and DCVJ are indicated. (B) Analysis of DCVJ fluorescence signal intensity upon binding to αSN monomers, oligomers, and fibrils. (C) Analysis of DCVJ binding to wt, A30P, E46K, and A53T αSN oligomers. (D) FTIR analysis of αSN fibrils prepared with ThT and DCVJ.

$$\log K_{O-M}^{\text{denaturant}} = \log K_{O-M}^{\text{water}} + m_{O-M}[\text{urea}] \quad (3)$$

This approach formally allows us to calculate the equilibrium constant (K_D^{water}) and free energy ($\Delta G_{D,\text{app}}^{\text{water}}$) in the absence of denaturant. However, we have refrained from calculating the free energy of dissociation and denaturation, since this assumes slow conversion between monomer and oligomer (which are separated during SDS-PAGE) and does not take into account changes in molecularity associated with oligomer denaturation. We do note that SDS present in the running buffer appears not to destabilize oligomers significantly, since the same monomer−oligomer distribution was obtained independent of SDS up to 3% SDS (see Results).

pH stability. The αSN oligomers were diluted into buffer with preadjusted pH to obtain a final protein concentration of 28 μM. The samples were incubated at room temperature for 24 h and then analyzed by SDS-PAGE. For pH 3−6, phosphate−citrate buffer was used (citric acid, dibasic sodium phosphate). For pH 9−11, glycine−NaOH buffer was used, while PBS buffer was used for pH 6−9.

Transmission Electron Microscopy (TEM). Ten microliters of 0.5 mg/mL (35 μM) αSN in PBS buffer (pH 7.4) was transferred to a 400-mesh carbon-coated, glow-discharged grid for 30 s. The grids were washed twice with a drop of doubly distilled water, stained with 1% uranyl acetate and blotted dry on filter paper. The samples were imaged on a transmission electron microscope (Philips CM100 Bio, Philips/FEI Corporation, Eindhoven, The Netherlands) operating at 80 kV.

Dynamic Light Scattering (DLS). DLS measurements were performed on a Zetasizer NANO ZS (Malvern Instruments Ltd., Worcestershire, U.K.) instrument. The oligomers were scanned in disposable, solvent resistant microcuvettes (Malvern Instruments Ltd., Worcestershire, UK) at 28 μM (αSN monomer equivalents). For each sample, 5 scans were acquired and averaged.

Small-Angle X-ray Scattering. Data were collected and analyzed as previously described.[25] Briefly, purified oligomers were measured on the flux- and background-optimized NanoSTAR SAXS instrument from Bruker,[72] with 60 min acquisition time for the oligomers. Buffer background was measured for the same time period. Background subtraction

dx.doi.org/10.1021/bi5007833 | Biochemistry 2014, 53, 6252−6263

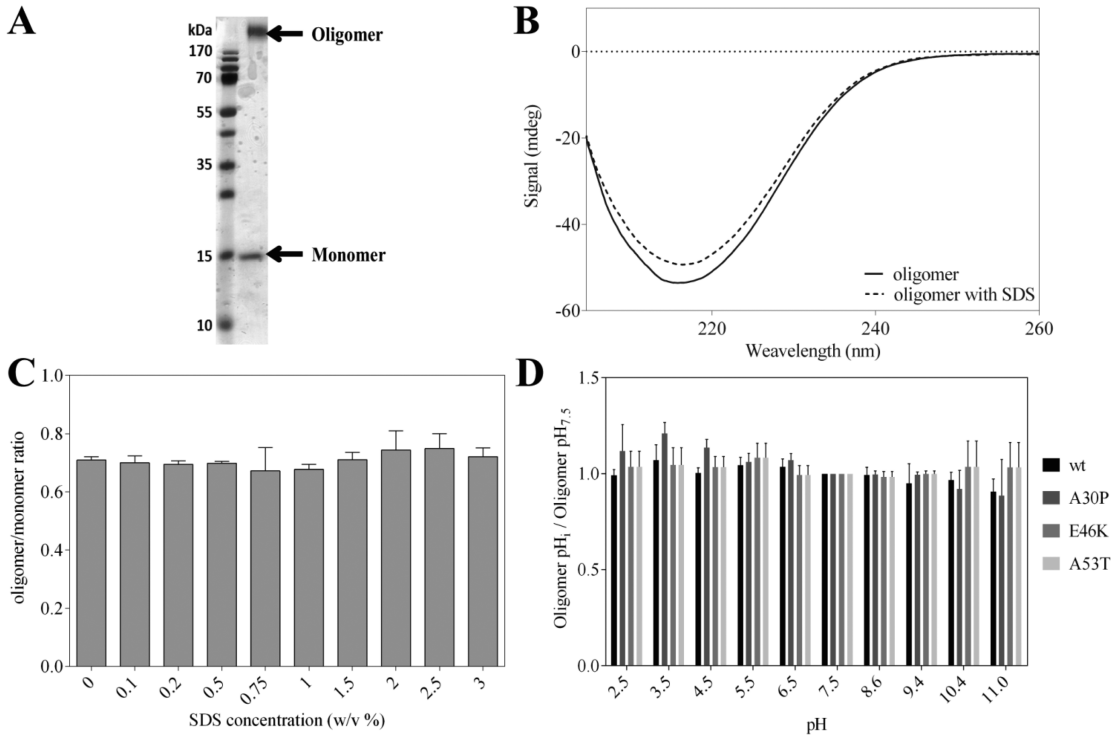

Figure 3. Analysis of oligomer population by SDS-PAGE. (A) Separation of oligomer and monomer αSN by SDS-PAGE. (B) CD spectra of αSN oligomer in PBS buffer (straight line) and in PBS buffer containing 3% SDS (dashed line). (C) Stability of wt αSN oligomer with increasing SDS concentration. Oligomer to monomer ratio at different concentrations of SDS in the sample. For each data column, the average of triplicates is shown with standard deviation on error bars. (D) Stability of wt, A30P, E46K, and A53T αSN oligomers between pH 2.5 and 11. Data are presented as a ratio of oligomer quantity in analyzed pH to oligomer amount in pH 7.5. For each data column, an average of triplicates is shown with standard deviation indicated by error bars.

and conversion to absolute scale was done with the SUPERSAXS program package (Oliveira, C. L. P., and Pedersen, J. S., unpublished), and water was used as a calibration standard. The intensity is displayed as a function of the modulus of the scattering vector $q = 4\pi \sin(\theta)/\lambda$, where $\lambda = 1.54$ Å is the wavelength and 2θ is the scattering angle. The oligomer data were fitted to the previously proposed model, where part of the protein forms a rather compact ellipsoidal core while the remaining flexible parts project randomly into the solution.[25]

RESULTS

The αSN Oligomer Is Present from the Beginning of the Fibrillization Process. We have previously used SAXS to show that an oligomer is present in freshly dissolved αSN and has disappeared as a separate soluble species by the time fibrillization is complete.[2] In principle, this may be caused by transformation to either monomers, fibrils, or higher aggregates coexisting with amyloid fibrils. Here we examine the appearance of the αSN oligomer in more detail by SEC analysis. During fibrillization (900 rpm shaking of 12 mg/mL αSN at 37 °C in PBS buffer), the oligomer population increases slowly over time, and a small but significant shift in its retention peak centroid from 23 min at 1 h incubation to 22.5 min at 4 h incubation (Figure 1A) occurs. After 4 h incubation, the retention time of the oligomer peak no longer shifts. This indicates that the oligomer grows slightly in size over the first 4 h. The fraction of larger aggregates, eluting in the void volume of the column, starts to increase after ca. 6 h (Figure 1A, inset).

The Shape of the Observed Oligomer Resembles a Prolate Ellipsoid. The αSN oligomer, examined in the present work, resembles the ellipsoidal oligomer observed in previous studies.[2,25,73] TEM of αSN wt oligomers reveals a round shape (Figure 1B), with a diameter of 13.9 ± 1.6 nm. The morphology of the oligomer is not changed by the concentration step in the purification of the oligomer (Figure 1C). We also investigate the structure of A30P, E46K, and A53T αSN oligomers in comparison to wt oligomers[25] using SAXS (Figure 1D, Table 1). All four data sets could be fit well with the model proposed earlier, consisting of a rather compact prolate core with a number of flexible chains protruding from the surface into the solution. When the model is fitted to the SAXS data, the absolute scale of the data determines the aggregation numbers, whereas the q dependence determines the size and the shape of the particles and distribution of protein in, respectively, the central part and the diffuse outer shell. The dimensions of the mutants are similar to that of wt αSN, but they seem slightly larger than wt, in the overall order E46K < A30P < A53T with respect to the dimensions of the core as determined from the fitting. At the same time, the fraction of flexible structure decreases. The number of monomers per oligomer was fixed to the aggregation numbers calculated from the forward scattering and the concentration. The aggregation numbers are similar, indicating that the slight increase in size might be caused by a less compact packing of the protein.

DCVJ Can Be Used as a Probe for αSN Oligomers. The oligomer identified in the early hours of the fibrillization process binds the dye ANS, indicating exposure of a hydrophobic surface in the oligomer.[74,75] However, this dye

dx.doi.org/10.1021/bi5007833 | Biochemistry 2014, 53, 6252−6263

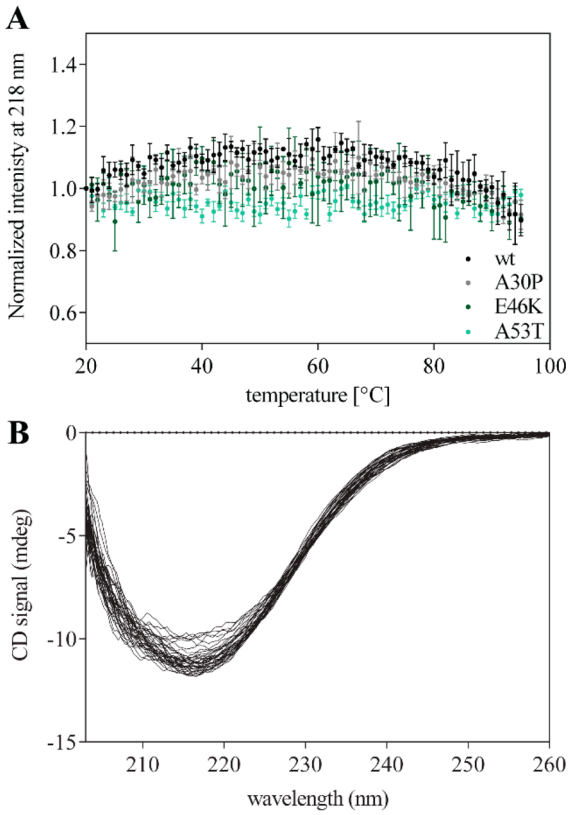

Figure 4. Thermal stability of αSN oligomers. (A) CD thermal scans from 20 to 95 °C of wt (black), A30P (gray), E46K (green) and A53T (light green) αSN oligomers. The normalized CD signal at 218 nm is shown. For each variant of αSN the average of triplicates is shown with standard deviation on error bars. (B) CD wavelength scans from 4 to 96 °C taken every 2 °C. No significant change in spectra suggest no disruption of the oligomer's secondary structure.

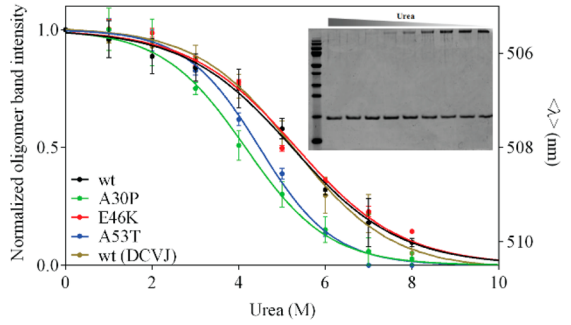

Figure 5. Dissociation of αSN oligomer measured using urea and SDS-PAGE. Oligomer band intensity (left *Y* axis) and average emission wavelength value, obtained from DCVJ fluorescence scans (right *Y* axis), plotted versus urea concentration (points) and fitting to two-state dissociation model (lines) for wt, A30P, E46K, and A53T αSN oligomer. (Inset) SDS-PAGE gel image showing decreasing oligomer band intensity with increasing urea concentration.

is not oligomer specific, because it also binds to αSN fibrils. The dye DCVJ has previously been used to detect prefibrillar oligomers of TTR.[76] We here use DCVJ as a dye to detect prefibrillar oligomers of αSN. The increase in the fluorescence signal of DCVJ coincides with the occurrence of an oligomer, detected by SEC, during the lag-phase and the exponential growth phase of αSN fibrillization (Figure 2A). The DCVJ fluorescence signal declines to approximately half of the maximum level at the same time as the ThT fibrillization signal reaches a plateau. This indicates that DCVJ binds to an intermediate αSN species that appears during the lag-phase and either disappears or rearranges during the fibrillization process. To further confirm that DCVJ recognizes αSN oligomers, the fluorescence emission spectra of DCVJ in the presence of various αSN species was recorded. The strongest signal was recorded in the presence of αSN oligomers (Figure 2B), though fibrils also elicited a significant signal. Furthermore, the same level of DCVJ fluorescence intensity is observed for purified oligomers of αSN mutants A30P, E46K, and A53T (Figure 2C). DCVJ binding does not alter the secondary structure of the resulting fibrils (Figure 2D). DCVJ also detects the formation of oligomers of αSN mutants A30P, E46K, and A53T, which in all cases lead to a rise and subsequent decline in DCVJ signal during the elongation phase of fibrillization, similar to wt αSN (data not shown).

αSN Oligomer Structure Is Resistant to Significant Changes in pH and Temperature. It was possible to estimate the population of oligomers from SDS-PAGE. Gels showed both a band corresponding to monomeric αSN (15 kDa) and a band migrating at >170 kDa (Figure 3A). SDS does not significantly affect oligomer stability (Figure 3B). Even in the presence of 3% SDS, the oligomer is still stable and its β-sheet-rich secondary structure is not significantly affected (Figure 3C). This made it possible for us to investigate the stability of the wt and mutant αSN oligomer over pH 2.5−11. Remarkably, both wt and mutant oligomers remain equally stable to dissociation over this entire pH range, indicating that titratable electrostatic interactions are not critical for oligomer stability (Figure 3D).

The thermal stability of the oligomer was tested using CD spectroscopy. Wavelength scans at 2 °C intervals from 4 to 95 °C reveal no major rearrangement in the secondary structure of the αSN oligomer (Figure 4). This indicates that the oligomer is thermally stable up to at least 95 °C. Thermal scans of A30P, E46K, and A53T αSN oligomers show identical thermal robustness (Figure 4). Even differential scanning calorimetry, which allows us to scan up to 120 °C, shows no transitions with ∼0.4 mg/mL αSN oligomer (data not shown). Thus, the αSN oligomer is thermally stable up to 120 °C. Moreover the secondary structure of oligomer cooled to 20 °C after heating to 100 °C is the same as that before temperature treatment, showing that no irreversible conformational changes occur.

αSN Oligomers Only Dissociate at Molar Concentrations of Urea. The stability of the αSN oligomer was tested

Table 2. Apparent Stability of αSN Oligomers Determined by Urea Denaturation Using SDS-PAGE and (for wt) DCVJ Fluorescence

	wt[a]	A30P[a]	E46K[a]	A53T[a]	wt (DCVJ)[b]
$m_{O\text{-}M}$[c]	0.352 ± 0.019	0.451 ± 0.028	0.354 ± 0.030	0.507 ± 0.033	0.384 ± 0.061
$den_{50\%}$ (M)[c]	5.226 ± 0.073	4.150 ± 0.068	5.321 ± 0.113	4.472 ± 0.063	5.268 ± 0.201

[a]Based on dissociation on SDS-PAGE gels. [b]Based on changes in DCVJ fluorescence. [c]Parameters obtained by fitting data to eq 2.

dx.doi.org/10.1021/bi5007833 | *Biochemistry* 2014, 53, 6252−6263

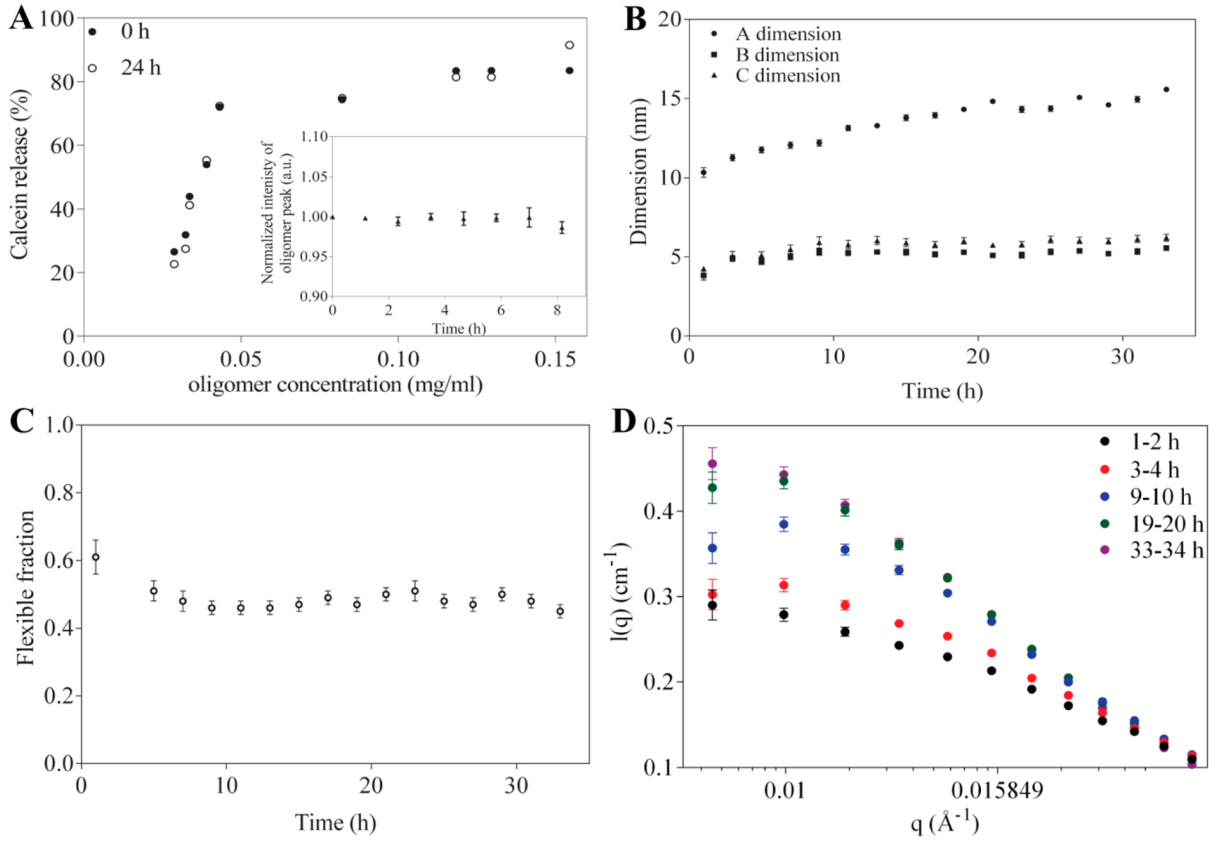

Figure 6. Stability of wt αSN oligomers over time. (A) Calcein release from phospholipid vesicles by oligomers at time zero after preparation (full circle) and after 24 h of incubation (empty circle). (Inset) SEC analysis of oligomer sample during 8 h of incubation presented as intensity of oligomer peak on chromatogram (triangles). (B) Change in oligomer dimensions obtained from SAXS analysis of oligomers incubated at 37 °C for 34 h. (C) Flexible fraction of protein chain obtained from SAXS analysis of oligomers incubated at 37 °C for 34 h. (D) Change in scattering intensity during incubation. Arrow indicates passage of time.

using urea denaturation followed by SDS-PAGE (Figure 5, inset). Quantifying the relative oligomer population by SDS-PAGE and plotting the oligomer concentration versus urea concentration, we observe a sigmoidal curve analogous to the equilibrium unfolding of compact monomeric proteins (Figure 5). Accordingly we analyze the curves by the formalism associated with monomeric protein stability,[70,71] though we stress that these values only yield apparent stability values, which merely serve a comparative purpose. The wt αSN oligomer has a dissociation midpoint of 5.2 ± 0.1 M urea (Table 2). Comparable results were obtained with the other mutants (Figure 5, Table 2).

Furthermore, we monitored urea denaturation of the oligomer in solution (rather than SDS-PAGE) using DCVJ as a reporter probe. The obtained midpoint of denaturation (5.3 ± 0.3 M urea, Figure 5, Table 2) are both consistent with the values obtained from the SDS-PAGE analysis, confirming DCVJ's ability to monitor oligomer population as well as the limited impact of SDS on oligomer stability.

αSN Oligomers Do Not Revert to Monomers over Several Days of Incubation. We next investigated oligomer stability over time. Overnight storage at 4 °C shows no reduction in the high membrane permeabilization activity of oligomers (Figure 6A). This indicates that the potential to interact with lipid vesicles did not change by overnight incubation and that no dissociation occurs at this low temperature. We observe similar results for samples incubated at increasing temperature (37 °C), where the amount of αSN oligomer remains constant over 9 h, according to SEC (Figure 6A, inset). This indicates that over this period of time no significant dissociation of the αSN oligomer occurs. Furthermore, DCVJ fluorescence in the presence of αSN oligomers remains constant over 5 days, ruling out dissociation to monomers (data not shown). SAXS data also indicate no dissociation of oligomers. In contrast, the oligomers increase in all dimensions; the major *A* dimension of the central part of the oligomer increases more slowly than the dimension in the other two directions, but they all increase by ca. 50% over $1^1/_2$ days (Figure 6B,C). However, our SAXS data are ensemble-averaged values and do not necessarily mean that the individual oligomers gradually increase in size. Rather, the increases in intensity for low *q* values could also indicate that aggregation to higher order species is occurring (Figure 6D). This is investigated further below.

αSN Oligomers Aggregate to Larger Structures during Prolonged Incubation. To verify that the oligomer indeed is still present in the sample after prolonged incubation at 37 °C, the morphology of the species present in the samples at various time points was examined by TEM (Figure 7). The fresh sample consists mostly of round species with small amounts of larger aggregates. After 3 days of incubation, the round species start to associate to two types of larger aggregates. The first, highly populated, type consists of agglomerated round-shaped oligomers forming worm-like structures (Figure 7, zoomed square). A second minor population consists of straight short fibrils. The individual

dx.doi.org/10.1021/bi5007833 | *Biochemistry* 2014, 53, 6252−6263

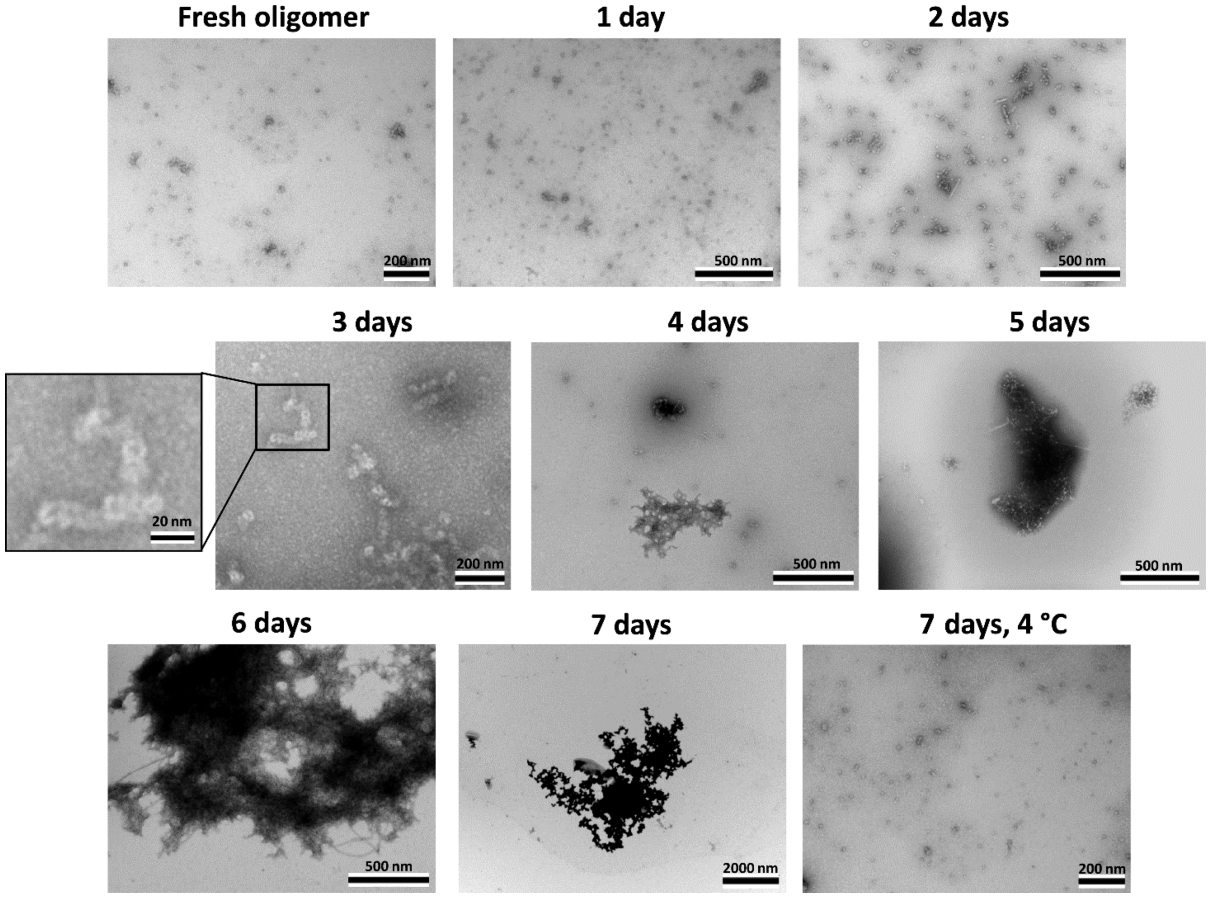

Figure 7. TEM imaging of wt αSN oligomers incubated at 37 °C for 1 week. Samples were imaged every 24 h. In addition the sample incubated for 1 week at 4 °C is presented. Magnification of worm-like aggregates formed by round-shaped αSN oligomers is presented for a sample aggregated for 3 days.

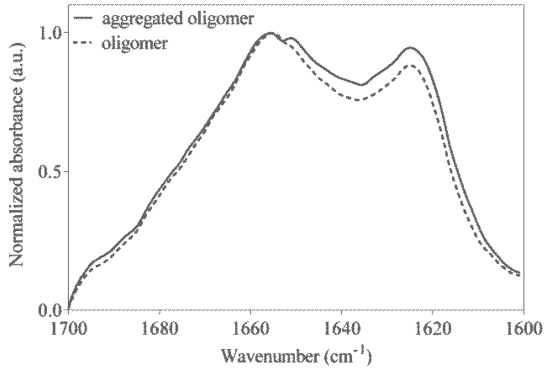

Figure 8. Comparison of secondary structure of oligomers and aggregates formed by oligomers using FTIR.

oligomers disappear after 5 days. Interestingly, after 1 week of incubation at 4 °C, no significant aggregation can be seen in the oligomer sample. Moreover the secondary structure of aggregates after 5 days of incubation is unchanged (Figure 8). DLS reveals three major species in the different samples, namely, small (diameter <40 nm), medium (diameter 40−250 nm), and large aggregates (diameter >250 nm) (Figure 9A). Importantly, the diameters of the three different species do not change significantly over time. This suggests that these three size classes represent aggregates that each consist of a relatively constant numbers of oligomers, which in turn supports our theory that the oligomers do not dissociate back to monomers but rather join together to form larger aggregates. Inspection of the derived count rates in the samples further confirms aggregation process (Figure 9B), and the size distribution reveals that after 4 days of incubation the small aggregates have disappeared (Figure 9A). This is consistent with the results obtained using TEM imaging. Furthermore, DLS data confirm that αSN oligomers incubated at 4 °C do not aggregate into larger aggregates but rather consist of single oligomers with small amount of medium sized aggregates (Figure 9 A,B).

DISCUSSION

αSN Oligomers Can Be Detected by DCVJ Fluorescence. There are few known fluorescent probes that can be used to detect αSN fibrils in addition to the commonly used ThT.[77] ANS has been used both to detect fibrils[78,79] and oligomers.[74,75] Fluorescence polarization, when combined with a suitable amyloid dye, allows monitoring of the fibrillization process and detection of oligomeric species.[80] Conformationally specific antibodies may also be used[73] but remain impractical for real-time measurements. However, we have found that the DCVJ fluorophore, which was previously used for detection of TTR aggregates,[63] detects αSN oligomers. Although DCVJ is not exclusively specific for oligomers, the increase in its fluorescence signal in the presence of αSN oligomers is around 2- and 4-fold larger than the corresponding increases for fibrils and monomers, respectively. DCVJ is a molecular rotor containing a fluorescent julolidine group and a dicyano group responsible for self-quenching. This type of

dx.doi.org/10.1021/bi5007833 | Biochemistry 2014, 53, 6252−6263

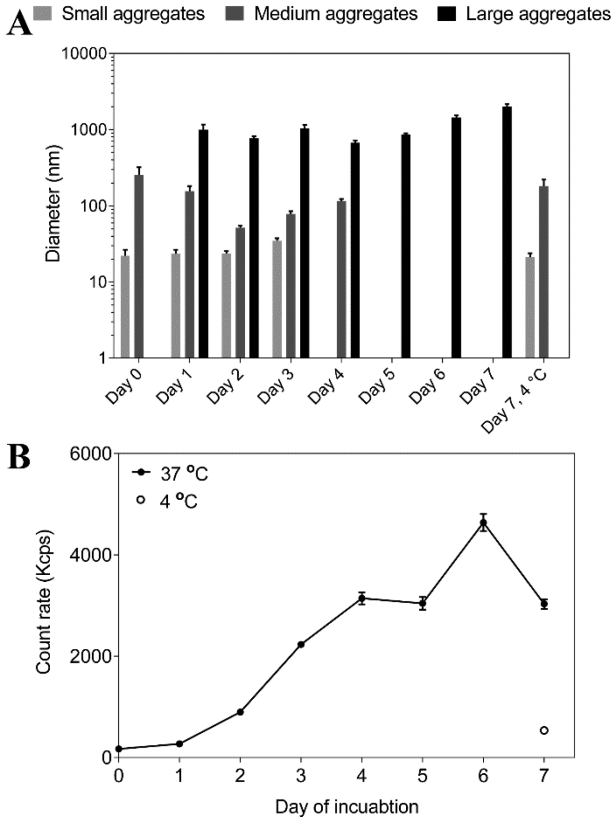

Figure 9. DLS analysis of wt αSN oligomers aggregation. (A) Size distribution of wt αSN oligomers incubated at 37 °C for 1 week. Samples were analyzed every 24 h. In addition the sample incubated for 1 week in 4 °C is presented. Observed aggregates are divided into three sections: small (diameter <40 nm), medium (diameter 40 nm −250 nm) and large aggregates (diameter >250 nm). (B) Derived count rates of analyzed samples for each day of incubation.

quenching makes it sensitive to intrinsic rotational relaxation, which is decreased upon binding to aggregated species. DCVJ's preference for αSN oligomers may be caused by intercalation of the DCVJ molecule into the oligomer cavity, leading to a greater decrease in intrinsic rotational relaxation than upon binding to fibrils. Interestingly, DCVJ fluorescence peaks sharply at 5 h, although the oligomer population remains relatively constant in this time range. We speculate that DCVJ may bind preferentially to the later oligomeric species (rather than the initial oligomeric species), which elutes slightly later on the SEC column (cf. the small shift in oligomer retention time during the first 2 h in Figure 1A, inset).Importantly, DCVJ does not appear to alter the secondary structure or stability of oligomeric αSN species upon binding and binds in a similar fashion to oligomers of αSN mutants, making it a valid probe for future studies.

The Oligomer Appears during the Lag Phase in the Fibrillization Process. TEM images and SAXS studies reveal an αSN oligomer with the same shape as the previously described ellipsoid oligomers.[2] SEC and DCVJ fluorescence indicate that the oligomer is present in the fibrillating sample during the lag phase and exponential growth phase. We are not able to detect the oligomers after the fibrillization process has reached a plateau, which might suggest that they are intermediate species in fibril formation. However, further aggregation steps will affect both SEC (due to limits in the size of aggregates that can enter the chromatography resin) and DCVJ fluorescence (due to depletion of binding sites). Therefore, the drop in the signal might also occur due to the assembly of larger species or formation of amorphous aggregates.

αSN Oligomers Assemble into Larger Aggregates and Do Not Revert to Monomers. The isolated oligomers are remarkably stable and do not dissociate into monomers. Their membrane permeabilization properties and levels of association are unchanged after a day of incubation at 4 or 37 °C. Nor do we observe a decrease in DCVJ signal upon incubation of oligomers at 37 °C for 5 days. However, DLS and TEM reveal that incubation at 37 °C leads predominantly to linearly associated oligomers, as well as a small amount of conventional fibrillar structures. This oligomer association does not occur upon incubation at 4 °C, indicating that the process is highly temperature-dependent. Both types of association are likely to decrease the amount of flexible structure in the oligomer through the formation of quaternary contacts, consistent with the overall increase in dimensions and decrease in flexible regions revealed by our SAXS studies.

The subject of how the fibrils are formed remains outside the scope of the present investigation, but we note that it is very unlikely that the fibrils are made solely from residual monomers in the sample. According to SEC-MALS, the residual monomer is present at concentrations more than 20 times lower than the one used in fibrillization assays. Furthermore, the solution is kept quiescent, and αSN incubated without agitation requires months to fibrillate.[81] Additionally, our recent study of the dynamics of αSN oligomers using hydrogen−deuterium exchange mass spectrometry revealed that their population is not homogeneous and two distinct oligomeric species are present in the purified sample.[60] The population of the major species remains constant over time. In contrast, the minor oligomer is in dynamic equilibrium with αSN monomers, leading to rapid exchange of otherwise protected amide protons. This makes it likely that the oligomer properties characterized in this study primarily represent the abundant type of the oligomer. We also observe that prolonged incubation of purified oligomers leads to formation of a small number of straight fibrils and a large population of "worm-like" aggregates. Based on these observations, we suggest that the minor αSN oligomer partially dissociates into monomers, which then elongate this oligomer, leading to straight fibrils. Effectively this makes the minor species an on-pathway structure to fibril formation. In contrast, the major oligomer neither dissociates nor interacts with monomers (formed due to dissociation of the first type of oligomer) and forms "worm-like" amorphous aggregates, suggesting that it is an off-pathway structure to the fibrillization process. The lack of interaction with monomers has been confirmed by independent studies.[25]

αSN Oligomers Are Very Stable and Are Not Easily Altered by Changes in Environment. Our data demonstrate that αSN oligomers are far more stable than we would expect for partially folded aggregated states with extensive amounts of denatured structure. Neither heating to extreme temperatures nor large changes in pH were able to dissociate the oligomers back to monomers or modify their structure as oligomers. They are not affected by reducing conditions used during SDS-PAGE and even preincubation in up to 3% SDS was not able to dissolve or alter the structure of αSN oligomers. Furthermore, the oligomers are also robust to urea denaturation; concentrations in excess of 5 M are needed to reach the midpoint of dissociation to monomers.

dx.doi.org/10.1021/bi5007833 | *Biochemistry* 2014, 53, 6252−6263

Oligomers' neuronal toxicity[5,46−49] make them an extremely important target for treatment of PD. The very high stability of αSN oligomers indicates that drug development should be aimed at surface passivation or inhibition of their formation rather than simple structure disruption, as is confirmed by previously reported inhibition of αSN oligomers' toxicity by compounds like curcumin,[82] geldanamycin (and its derivatives)[83−85] and EGCG.[86,87]

AUTHOR INFORMATION

Corresponding Author

*Daniel E. Otzen. Tel: + 45 20 72 52 38. E-mail: dao@inano.au.dk.

Present Addresses

∥S.B.N.: Arla Foods Ingredients Group P/S, Sønderupvej 26, DK - 6920 Videbæk, Denmark.

⊥N.L.: Department of Protein Biophysics and Formulation, Novo Nordisk A/S, 2760 Måløv, Denmark

Funding

W.P., M.A., N.L., S.B.N., and D.E.O. are supported by the Michael J. Fox Foundation, the Danish Research Council (Industrial Post-doc and The Danish Council for Independent Research|Natural Sciences), and the Danish Research Foundation (inSPIN). J.D.K. and J.S.P. acknowledge LUNDBECKFONDEN for financial support as well as from The Danish Council for Independent Research|Natural Sciences.

Notes

The authors declare no competing financial interest.

ABBREVIATIONS

αSN, α-synuclein; CBB, Coomassie Brilliant Blue; CD, circular dichroism; DCVJ, 4-(dicyanovinyl)julolidine; DLS, dynamic light scattering; FTIR, Fourier-transform infrared; NDs, neurodegenerative diseases; PBS, phosphate buffered saline; PD, Parkinson's disease; SDS-PAGE, sodium dodecyl sulfate polyacrylamide gel electrophoresis; SEC, size-exclusion chromatography; SDS, sodium dodecyl sulfate; TEM, transmission electron microscopy; ThT, thioflavin T; TTR, transthyretin; wt, wild-type; SAXS, small-angle X-ray scattering

REFERENCES

(1) Chiti, F., and Dobson, C. M. (2006) Protein misfolding, functional amyloid, and human disease. *Annu. Rev. Biochem. 75*, 333−366.

(2) Giehm, L., Svergun, D. I., Otzen, D. E., and Vestergaard, B. (2011) Low-resolution structure of a vesicle disrupting α-synuclein oligomer that accumulates during fibrillation. *Proc. Natl. Acad. Sci. U.S.A. 108*, 3246−3251.

(3) Lashuel, H. A., Hartley, D., Petre, B. M., Walz, T., and Lansbury, P. T., Jr. (2002) Neurodegenerative disease: Amyloid pores from pathogenic mutations. *Nature 418*, 291.

(4) Conway, K. A., Lee, S. J., Rochet, J. C., Ding, T. T., Williamson, R. E., and Lansbury, P. T., Jr. (2000) Acceleration of oligomerization, not fibrillization, is a shared property of both alpha-synuclein mutations linked to early-onset Parkinson's disease: implications for pathogenesis and therapy. *Proc. Natl. Acad. Sci. U.S.A. 97*, 571−576.

(5) Winner, B., Jappelli, R., Maji, S. K., Desplats, P. A., Boyer, L., Aigner, S., Hetzer, C., Loher, T., Vilar, M., Campioni, S., Tzitzilonis, C., Soragni, A., Jessberger, S., Mira, H., Consiglio, A., Pham, E., Masliah, E., Gage, F. H., and Riek, R. (2011) In vivo demonstration that alpha-synuclein oligomers are toxic. *Proc. Natl. Acad. Sci. U.S.A. 108*, 4194−4199.

(6) Walsh, D. M., and Selkoe, D. J. (2007) A beta oligomers - a decade of discovery. *J. Neurochem. 101*, 1172−1184.

(7) Lesne, S., Koh, M. T., Kotilinek, L., Kayed, R., Glabe, C. G., Yang, A., Gallagher, M., and Ashe, K. H. (2006) A specific amyloid-beta protein assembly in the brain impairs memory. *Nature 440*, 352−357.

(8) Nilsberth, C., Westlind-Danielsson, A., Eckman, C. B., Condron, M. M., Axelman, K., Forsell, C., Stenh, C., Luthman, J., Teplow, D. B., Younkin, S. G., Naslund, J., and Lannfelt, L. (2001) The 'Arctic' APP mutation (E693G) causes Alzheimer's disease by enhanced Abeta protofibril formation. *Nat. Neurosci. 4*, 887−893.

(9) Bernstein, S. L., Dupuis, N. F., Lazo, N. D., Wyttenbach, T., Condron, M. M., Bitan, G., Teplow, D. B., Shea, J. E., Ruotolo, B. T., Robinson, C. V., and Bowers, M. T. (2009) Amyloid-beta protein oligomerization and the importance of tetramers and dodecamers in the aetiology of Alzheimer's disease. *Nat. Chem. 1*, 326−331.

(10) Ward, S. M., Himmelstein, D. S., Lancia, J. K., and Binder, L. I. (2012) Tau oligomers and tau toxicity in neurodegenerative disease. *Biochem. Soc. Trans. 40*, 667−671.

(11) Volles, M. J., Lee, S. J., Rochet, J. C., Shtilerman, M. D., Ding, T. T., Kessler, J. C., and Lansbury, P. T., Jr. (2001) Vesicle permeabilization by protofibrillar alpha-synuclein: Implications for the pathogenesis and treatment of Parkinson's disease. *Biochemistry 40*, 7812−7819.

(12) Hill, S. E., Robinson, J., Matthews, G., and Muschol, M. (2009) Amyloid protofibrils of lysozyme nucleate and grow via oligomer fusion. *Biophys. J. 96*, 3781−3790.

(13) Vestergaard, B., Groenning, M., Roessle, M., Kastrup, J. S., van de Weert, M., Flink, J. M., Frokjaer, S., Gajhede, M., and Svergun, D. I. (2007) A helical structural nucleus is the primary elongating unit of insulin amyloid fibrils. *PLoS Biol. 5*, No. e134.

(14) Lorenzen, N., Cohen, S. I. A., Nielsen, S. B., Herling, T. W., Christiansen, G., Dobson, C. M., Knowles, T. P. J., and Otzen, D. (2012) Role of Elongation and Secondary Pathways in S6 Amyloid Fibril Growth. *Biophys. J. 102*, 2167−2175.

(15) Kardos, J., Yamamoto, K., Hasegawa, K., Naiki, H., and Goto, Y. (2004) Direct measurement of the thermodynamic parameters of amyloid formation by isothermal titration calorimetry. *J. Biol. Chem. 279*, 55308−55314.

(16) Kim, H. J., Chatani, E., Goto, Y., and Paik, S. R. (2007) Seed-dependent accelerated fibrillation of alpha-synuclein induced by periodic ultrasonication treatment. *J. Microbiol. Biotechnol. 17*, 2027−2032.

(17) Morris, A. M., Watzky, M. A., and Finke, R. G. (2009) Protein aggregation kinetics, mechanism, and curve-fitting: A review of the literature. *Biochim. Biophys. Acta 1794*, 375−397.

(18) Knowles, T. P., Fitzpatrick, A. W., Meehan, S., Mott, H. R., Vendruscolo, M., Dobson, C. M., and Welland, M. E. (2007) Role of intermolecular forces in defining material properties of protein nanofibrils. *Science 318*, 1900−1903.

(19) Collins, S. R., Douglass, A., Vale, R. D., and Weissman, J. S. (2004) Mechanism of prion propagation: Amyloid growth occurs by monomer addition. *PLoS Biol. 2*, No. e321.

(20) Jain, S., and Udgaonkar, J. B. (2011) Defining the pathway of worm-like amyloid fibril formation by the mouse prion protein by delineation of the productive and unproductive oligomerization reactions. *Biochemistry 50*, 1153−1161.

(21) Necula, M., Kayed, R., Milton, S., and Glabe, C. G. (2007) Small molecule inhibitors of aggregation indicate that amyloid beta oligomerization and fibrillization pathways are independent and distinct. *J. Biol. Chem. 282*, 10311−10324.

(22) Souillac, P. O., Uversky, V. N., Millett, I. S., Khurana, R., Doniach, S., and Fink, A. L. (2002) Elucidation of the molecular mechanism during the early events in immunoglobulin light chain amyloid fibrillation. Evidence for an off-pathway oligomer at acidic pH. *J. Biol. Chem. 277*, 12666−12679.

(23) Gellermann, G. P., Byrnes, H., Striebinger, A., Ullrich, K., Mueller, R., Hillen, H., and Barghorn, S. (2008) Abeta-globulomers are formed independently of the fibril pathway. *Neurobiol. Dis. 30*, 212−220.

(24) Hong, D. P., Han, S., Fink, A. L., and Uversky, V. N. (2011) Characterization of the non-fibrillar alpha-synuclein oligomers. *Protein Pept. Lett. 18*, 230−240.
(25) Lorenzen, N., Nielsen, S. B., Buell, A. K., Kaspersen, J. D., Arosio, P., Vad, B. S., Paslawski, W., Christiansen, G., Valnickova-Hansen, Z., Andreasen, M., Enghild, J. J., Pedersen, J. S., Dobson, C. M., Knowles, T. J., and Otzen, D. E. (2014) The role of stable α-synuclein oligomers in the molecular events underlying amyloid formation. *J. Am. Chem. Soc. 136*, 3859−3868.
(26) Stefanis, L. (2012) alpha-Synuclein in Parkinson's disease. *Cold Spring Harbor Perspect. Med. 2*, No. a009399.
(27) Kruger, R., Kuhn, W., Muller, T., Woitalla, D., Graeber, M., Kosel, S., Przuntek, H., Epplen, J. T., Schols, L., and Riess, O. (1998) Ala30Pro mutation in the gene encoding alpha-synuclein in Parkinson's disease. *Nat. Genet. 18*, 106−108.
(28) Zarranz, J. J., Alegre, J., Gomez-Esteban, J. C., Lezcano, E., Ros, R., Ampuero, I., Vidal, L., Hoenicka, J., Rodriguez, O., Atares, B., Llorens, V., Gomez Tortosa, E., del Ser, T., Munoz, D. G., and de Yebenes, J. G. (2004) The new mutation, E46K, of alpha-synuclein causes Parkinson and Lewy body dementia. *Ann. Neurol. 55*, 164−173.
(29) Hamilton, B. A. (2004) alpha-Synuclein A53T substitution associated with Parkinson disease also marks the divergence of Old World and New World primates. *Genomics 83*, 739−742.
(30) Chartier-Harlin, M. C., Kachergus, J., Roumier, C., Mouroux, V., Douay, X., Lincoln, S., Levecque, C., Larvor, L., Andrieux, J., Hulihan, M., Waucquier, N., Defebvre, L., Amouyel, P., Farrer, M., and Destee, A. (2004) Alpha-synuclein locus duplication as a cause of familial Parkinson's disease. *Lancet 364*, 1167−1169.
(31) Singleton, A. B., Farrer, M., Johnson, J., Singleton, A., Hague, S., Kachergus, J., Hulihan, M., Peuralinna, T., Dutra, A., Nussbaum, R., Lincoln, S., Crawley, A., Hanson, M., Maraganore, D., Adler, C., Cookson, M. R., Muenter, M., Baptista, M., Miller, D., Blancato, J., Hardy, J., and Gwinn-Hardy, K. (2003) alpha-Synuclein locus triplication causes Parkinson's disease. *Science 302*, 841.
(32) Appel-Cresswell, S., Vilarino-Guell, C., Encarnacion, M., Sherman, H., Yu, I., Shah, B., Weir, D., Thompson, C., Szu-Tu, C., Trinh, J., Aasly, J. O., Rajput, A., Rajput, A. H., Stoessl, A. J., and Farrer, M. J. (2013) Alpha-synuclein p.H50Q, a novel pathogenic mutation for Parkinson's disease. *Mov. Disord. 28*, 811−813.
(33) Lesage, S., Anheim, M., Letournel, F., Bousset, L., Honore, A., Rozas, N., Pieri, L., Madiona, K., Durr, A., Melki, R., Verny, C., and Brice, A. (2013) G51D alpha-synuclein mutation causes a novel parkinsonian-pyramidal syndrome. *Ann. Neurol. 73*, 459−471.
(34) Chandra, S., Gallardo, G., Fernandez-Chacon, R., Schluter, O. M., and Sudhof, T. C. (2005) Alpha-synuclein cooperates with CSPalpha in preventing neurodegeneration. *Cell 123*, 383−396.
(35) Takenouchi, T., Hashimoto, M., Hsu, L. J., Mackowski, B., Rockenstein, E., Mallory, M., and Masliah, E. (2001) Reduced neuritic outgrowth and cell adhesion in neuronal cells transfected with human alpha-synuclein. *Mol. Cell. Neurosci. 17*, 141−150.
(36) Tsuboi, K., Grzesiak, J. J., Bouvet, M., Hashimoto, M., Masliah, E., and Shults, C. W. (2005) Alpha-synuclein overexpression in oligodendrocytic cells results in impaired adhesion to fibronectin and cell death. *Mol. Cell. Neurosci. 29*, 259−268.
(37) Bartels, T., Choi, J. G., and Selkoe, D. J. (2011) alpha-Synuclein occurs physiologically as a helically folded tetramer that resists aggregation. *Nature 477*, 107−110.
(38) Fauvet, B., Mbefo, M. K., Fares, M. B., Desobry, C., Michael, S., Ardah, M. T., Tsika, E., Coune, P., Prudent, M., Lion, N., Eliezer, D., Moore, D. J., Schneider, B., Aebischer, P., El-Agnaf, O. M., Masliah, E., and Lashuel, H. A. (2012) alpha-Synuclein in central nervous system and from erythrocytes, mammalian cells, and Escherichia coli exists predominantly as disordered monomer. *J. Biol. Chem. 287*, 15345−15364.
(39) Wang, W., Perovic, I., Chittuluru, J., Kaganovich, A., Nguyen, L. T., Liao, J., Auclair, J. R., Johnson, D., Landeru, A., Simorellis, A. K., Ju, S., Cookson, M. R., Asturias, F. J., Agar, J. N., Webb, B. N., Kang, C., Ringe, D., Petsko, G. A., Pochapsky, T. C., and Hoang, Q. Q. (2011) A soluble alpha-synuclein construct forms a dynamic tetramer. *Proc. Natl. Acad. Sci. U.S.A. 108*, 17797−17802.
(40) Dettmer, U., Newman, A. J., Luth, E. S., Bartels, T., and Selkoe, D. (2013) In vivo cross-linking reveals principally oligomeric forms of alpha-synuclein and beta-synuclein in neurons and non-neural cells. *J. Biol. Chem. 288*, 6371−6385.
(41) Binolfi, A., Theillet, F. X., and Selenko, P. (2012) Bacterial in-cell NMR of human alpha-synuclein: a disordered monomer by nature? *Biochem. Soc. Trans. 40*, 950−954.
(42) Coelho-Cerqueira, E., Carmo-Goncalves, P., Sa Pinheiro, A., Cortines, J., and Follmer, C. (2013) alpha-Synuclein as an intrinsically disordered monomer - fact or artefact? *FEBS J. 280*, 4915−4927.
(43) Weinreb, P. H., Zhen, W., Poon, A. W., Conway, K. A., and Lansbury, P. T., Jr. (1996) NACP, a protein implicated in Alzheimer's disease and learning, is natively unfolded. *Biochemistry 35*, 13709−13715.
(44) Spillantini, M. G., Crowther, R. A., Jakes, R., Hasegawa, M., and Goedert, M. (1998) alpha-Synuclein in filamentous inclusions of Lewy bodies from Parkinson's disease and dementia with lewy bodies. *Proc. Natl. Acad. Sci. U.S.A. 95*, 6469−6473.
(45) Fink, A. L. (1998) Protein aggregation: Folding aggregates, inclusion bodies and amyloid. *Folding Des. 3*, R9−23.
(46) Celej, M. S., Sarroukh, R., Goormaghtigh, E., Fidelio, G. D., Ruysschaert, J. M., and Raussens, V. (2012) Toxic prefibrillar alpha-synuclein amyloid oligomers adopt a distinctive antiparallel beta-sheet structure. *Biochem. J. 443*, 719−726.
(47) Cremades, N., Cohen, S. I., Deas, E., Abramov, A. Y., Chen, A. Y., Orte, A., Sandal, M., Clarke, R. W., Dunne, P., Aprile, F. A., Bertoncini, C. W., Wood, N. W., Knowles, T. P., Dobson, C. M., and Klenerman, D. (2012) Direct observation of the interconversion of normal and toxic forms of alpha-synuclein. *Cell 149*, 1048−1059.
(48) Outeiro, T. F., Putcha, P., Tetzlaff, J. E., Spoelgen, R., Koker, M., Carvalho, F., Hyman, B. T., and McLean, P. J. (2008) Formation of toxic oligomeric alpha-synuclein species in living cells. *PloS One 3*, No. e1867.
(49) Stockl, M. T., Zijlstra, N., and Subramaniam, V. (2013) Alpha-synuclein oligomers: an amyloid pore? Insights into mechanisms of alpha-synuclein oligomer-lipid interactions. *Mol. Neurobiol. 47*, 613−621.
(50) Lashuel, H. A., Overk, C. R., Oueslati, A., and Masliah, E. (2013) The many faces of alpha-synuclein: from structure and toxicity to therapeutic target. *Nat. Rev. Neurosci. 14*, 38−48.
(51) Kalia, L. V., Kalia, S. K., McLean, P. J., Lozano, A. M., and Lang, A. E. (2013) alpha-Synuclein oligomers and clinical implications for Parkinson disease. *Ann. Neurol. 73*, 155−169.
(52) Tsigelny, I. F., Sharikov, Y., Wrasidlo, W., Gonzalez, T., Desplats, P. A., Crews, L., Spencer, B., and Masliah, E. (2012) Role of alpha-synuclein penetration into the membrane in the mechanisms of oligomer pore formation. *FEBS J. 279*, 1000−1013.
(53) van Rooijen, B. D., Claessens, M. M., and Subramaniam, V. (2010) Membrane Permeabilization by Oligomeric alpha-Synuclein: In Search of the Mechanism. *PloS One 5*, No. e14292.
(54) van Rooijen, B. D., Claessens, M. M., and Subramaniam, V. (2009) Lipid bilayer disruption by oligomeric alpha-synuclein depends on bilayer charge and accessibility of the hydrophobic core. *Biochim. Biophys. Acta 1788*, 1271−1278.
(55) Polymeropoulos, M. H., Higgins, J. J., Golbe, L. I., Johnson, W. G., Ide, S. E., Di Iorio, G., Sanges, G., Stenroos, E. S., Pho, L. T., Schaffer, A. A., Lazzarini, A. M., Nussbaum, R. L., and Duvoisin, R. C. (1996) Mapping of a gene for Parkinson's disease to chromosome 4q21-q23. *Science 274*, 1197−1199.
(56) Spillantini, M. G., Schmidt, M. L., Lee, V. M., Trojanowski, J. Q., Jakes, R., and Goedert, M. (1997) Alpha-synuclein in Lewy bodies. *Nature 388*, 839−840.
(57) Polymeropoulos, M. H., Lavedan, C., Leroy, E., Ide, S. E., Dehejia, A., Dutra, A., Pike, B., Root, H., Rubenstein, J., Boyer, R., Stenroos, E. S., Chandrasekharappa, S., Athanassiadou, A., Papapetropoulos, T., Johnson, W. G., Lazzarini, A. M., Duvoisin, R. C., Di Iorio, G., Golbe, L. I., and Nussbaum, R. L. (1997) Mutation in

the alpha-synuclein gene identified in families with Parkinson's disease. *Science 276*, 2045−2047.
(58) Uversky, V. N. (2010) Mysterious oligomerization of the amyloidogenic proteins. *FEBS J. 277*, 2940−2953.
(59) Fandrich, M. (2012) Oligomeric intermediates in amyloid formation: structure determination and mechanisms of toxicity. *J. Mol. Biol. 421*, 427−440.
(60) Paslawski, W., Mysling, S., Thomsen, K., Jørgensen, T. J. D., and Otzen, D. E. (2014) Co-existence of two different α-synuclein oligomers with different core structures determined by Hydrogen/Deuterium Exchange Mass Spectrometry. *Angew. Chem., Int. Ed. Engl. 53*, 7560−7563, DOI: 10.1002/anie.201400491.
(61) Lorenzen, N., Nielsen, S. B., Yoshimura, Y., Andersen, C. B., Betzer, C., Vad, B. S., Kaspersen, J. D., Christiansen, G., Pedersen, J. S., Jensen, P. H., Mulder, F. A., and Otzen, D. E. (2014) How epigallocatechin gallate can inhibit α-synuclein oligomer toxicity *in vitro*. *J. Biol. Chem. 289*, 21299−21310, DOI: 10.1074/jbc.M114.554667.
(62) Lorenzen, N., Lemminger, L., Pedersen, J. N., Nielsen, S. B., and Otzen, D. E. (2013) The N-terminus of α-synuclein is essential for both monomeric and oligomeric interactions with membranes. *FEBS Lett. 588*, 497−502.
(63) Lindgren, M., Sorgjerd, K., and Hammarstrom, P. (2005) Detection and characterization of aggregates, prefibrillar amyloidogenic oligomers, and protofibrils using fluorescence spectroscopy. *Biophys. J. 88*, 4200−4212.
(64) Huang, C., Ren, G., Zhou, H., and Wang, C. C. (2005) A new method for purification of recombinant human alpha-synuclein in Escherichia coli. *Protein Expression Purif. 42*, 173−177.
(65) Giehm, L., Lorenzen, N., and Otzen, D. E. (2011) Assays for alpha-synuclein aggregation. *Methods 53*, 295−305.
(66) Giehm, L., and Otzen, D. E. (2010) Strategies to increase the reproducibility of protein fibrillization in plate reader assays. *Anal. Biochem. 400*, 270−281.
(67) Nesgaard, L., Vad, B., Christiansen, G., and Otzen, D. (2009) Kinetic partitioning between aggregation and vesicle permeabilization by modified ADan. *Biochim. Biophys. Acta 1794*, 84−93.
(68) Abramoff, M. D., Magelhaes, P. J., and Ram, S. J. (2004) Image Processing with ImageJ. *Biophotonics Int. 11*, 36−42.
(69) Royer, C. A., Mann, C. J., and Matthews, C. R. (1993) Resolution of the fluorescence equilibrium unfolding profile of trp aporepressor using single tryptophan mutants. *Protein Sci. 2*, 1844−1852.
(70) Pace, C. N. (1986) Determination and analysis of urea and guanidine hydrochloride denaturation curves. *Methods Enzymol. 131*, 266−279.
(71) Mogensen, J. E., Ibsen, H., Lund, J., and Otzen, D. E. (2004) Elimination of an off-pathway folding intermediate by a single point mutation. *Biochemistry 43*, 3357−3367.
(72) Pedersen, J. S. (2004) A flux- and background-optimized version of the NanoSTAR small-angle X-ray scattering camera for solution scattering. *J. Appl. Crystallogr. 37*, 368−380.
(73) Kayed, R., Head, E., Thompson, J. L., McIntire, T. M., Milton, S. C., Cotman, C. W., and Glabe, C. G. (2003) Common structure of soluble amyloid oligomers implies common mechanism of pathogenesis. *Science 300*, 486−489.
(74) Celej, M. S., Jares-Erijman, E. A., and Jovin, T. M. (2008) Fluorescent N-arylaminonaphthalene sulfonate probes for amyloid aggregation of alpha-synuclein. *Biophys. J. 94*, 4867−4879.
(75) Bolognesi, B., Kumita, J. R., Barros, T. P., Esbjorner, E. K., Luheshi, L. M., Crowther, D. C., Wilson, M. R., Dobson, C. M., Favrin, G., and Yerbury, J. J. (2010) ANS binding reveals common features of cytotoxic amyloid species. *ACS Chem. Biol. 5*, 735−740.
(76) Lindgren, M., Sörgjerd, K., and Hammarström, P. (2005) Detection and Characterization of Aggregates, Prefibrillar Amyloidogenic Oligomers, and Protofibrils Using Fluorescence Spectroscopy. *Biophys. J. 88*, 4200−4212.
(77) Ban, T., Hamada, D., Hasegawa, K., Naiki, H., and Goto, Y. (2003) Direct observation of amyloid fibril growth monitored by thioflavin T fluorescence. *J. Biol. Chem. 278*, 16462−16465.
(78) Dusa, A., Kaylor, J., Edridge, S., Bodner, N., Hong, D. P., and Fink, A. L. (2006) Characterization of oligomers during α-synuclein aggregation using intrinsic tryptophan fluorescence. *Biochemistry 45*, 2752−2760.
(79) Munishkina, L. A., Phelan, C., Uversky, V. N., and Fink, A. L. (2003) Conformational behavior and aggregation of α-synuclein in organic solvents: Modeling the effects of membranes. *Biochemistry 42*, 2720−2730.
(80) Luk, K. C., Hyde, E. G., Trojanowski, J. Q., and Lee, V. M. (2007) Sensitive fluorescence polarization technique for rapid screening of α-synuclein oligomerization/fibrillization inhibitors. *Biochemistry 46*, 12522−12529.
(81) Fink, A. L. (2006) The aggregation and fibrillation of α-synuclein. *Acc. Chem. Res. 39*, 628−634.
(82) Singh, P. K., Kotia, V., Ghosh, D., Mohite, G. M., Kumar, A., and Maji, S. K. (2013) Curcumin modulates α-synuclein aggregation and toxicity. *ACS Chem. Neurosci. 4*, 393−407.
(83) Putcha, P., Danzer, K. M., Kranich, L. R., Scott, A., Silinski, M., Mabbett, S., Hicks, C. D., Veal, J. M., Steed, P. M., Hyman, B. T., and McLean, P. J. (2010) Brain-permeable small-molecule inhibitors of Hsp90 prevent alpha-synuclein oligomer formation and rescue alpha-synuclein-induced toxicity. *J. Pharmacol. Exp. Ther. 332*, 849−857.
(84) McLean, P. J., Klucken, J., Shin, Y., and Hyman, B. T. (2004) Geldanamycin induces Hsp70 and prevents alpha-synuclein aggregation and toxicity in vitro. *Biochem. Biophys. Res. Commun. 321*, 665−669.
(85) Riedel, M., Goldbaum, O., Schwarz, L., Schmitt, S., and Richter-Landsberg, C. (2010) 17-AAG induces cytoplasmic alpha-synuclein aggregate clearance by induction of autophagy. *PloS One 5*, No. e8753.
(86) Ehrnhoefer, D. E., Bieschke, J., Boeddrich, A., Herbst, M., Masino, L., Lurz, R., Engemann, S., Pastore, A., and Wanker, E. E. (2008) EGCG redirects amyloidogenic polypeptides into unstructured, off-pathway oligomers. *Nat. Struct. Mol. Biol. 15*, 558−566.
(87) Grelle, G., Otto, A., Lorenz, M., Frank, R. F., Wanker, E. E., and Bieschke, J. (2011) Black tea theaflavins inhibit formation of toxic amyloid-β and α-synuclein fibrils. *Biochemistry 50*, 10624−10636.